Characterization of optical-aberration-induced lateral and axial image inhomogeneity in multiphoton microscopy

Vladimir A. Hovhannisyan
Ping-Jung Su
Chen Yuan Dong
National Taiwan University
Department of Physics
Taipei 106, Taiwan
E-mail: cydong@phys.ntu.edu.tw

Abstract. The effects of off-axis optical aberration in multiphoton microscopy and the resulting lateral and axial image inhomogeneity are investigated. The lateral inhomogeneity of the scanning field is demonstrated by second harmonic generation (SHG) imaging of fasciae and two-photon fluorescence (TPF) microscopy of thin fluorescent samples. Furthermore, refractive index mismatch-caused intensity attenuation of the TPF signal at central and peripheral regions of the scanning frame is measured using homogeneous 10-μM sulforhodamine B samples with refractive indexes of 1.33 and around 1.465. In addition to characterizing image field convexity, we also found that image resolution degrades away from the optical axis. These effects need to be accounted for in both qualitative and quantitative multphoton imaging applications. [DOI: 10.1117/1.2950314]

Keywords: multiphoton; fluorescence; second harmonic generation; spherical aberration; point spread function.

Paper 07478R received Dec. 1, 2007; revised manuscript received Feb. 5, 2008; accepted for publication Feb. 6, 2008; published online Jul. 24, 2008.

1 Introduction

Multiphoton laser scanning microscopy (MLSM) has been extensively used in biomedical research to yield 3-D images of biological specimens by scanning a focused, ultrafast laser source along the lateral and axial coordinates.[1] However, due to the nonlinear dependence of the signal strength on excitation intensity, the multiphoton excitation efficiency can be significantly affected by factors such as depolarization, phase front distortion, coherence degradation, and dispersion. Furthermore, laser beam quality can also be degraded by aberrations present in the imaging system and the refractive index mismatch (RIM)-induced spherical aberration between the sample and the focusing objective. As a result, spatial resolution, image penetration depth, signal intensity, and image contrast can be adversely affected.

Recent studies have paid considerable attention to the effects of RIM-induced spherical aberration in confocal and multiphoton imaging. With increasing imaging depths, spherical aberration was shown to reduce the excitation efficiency of two-photon fluorescence (TPF) and degrade spatial resolution in nonlinear and confocal microscopy.[2–8] In particular, it was found that for a high-numerical-aperture oil-immersion objective (NA 1.3), the point spread function (PSF) at an imaging depth of 90 μm was seven times larger than that found just below the surface of aqueous samples.[3] To correct the intensity attenuation of the reconstructed images, methodologies based on software (maximum likelihood estimation algorithms,[3] fast fourier transform (FFT)-based iterative method,[9] 2-D histogram,[10] estimations of intensity decay function,[11] spatially adaptive mean-weight filtering[12]) and hardware (two-view imaging,[13] objective correction collar,[14] adaptive optics[15,16]) were used. However, in most of these studies, the same degree of spherical aberration was assumed to occur across the scanned area at a given imaging depth. The effects of off-axis aberrations such as coma, astigmatism, and field curvature were not considered. In this study, we investigate the effects of optical aberration when imaging objects are positioned away from the optical axis. We aim to investigate quantitatively off-axis reduction of the spatial resolution and intensity at different imaging depths in the presence of RIM in the immersion liquid-specimen system. To the best of our knowledge, lateral image inhomogeneity in multiphoton microscopy has not been investigated. Such an effect, if present, can lead to incorrect interpretations of multiphoton imaging results in both qualitative and quantitative manners. To verify this hypothesis, we qualitatively demonstrate and quantitatively determine the effects of optical aberration in multiphoton imaging of specimens located away from the optical axis by the second harmonic generation (SHG) imaging of collagen-containing fasciae and two-photon imaging of uniform sulforhodamine B (SRB) in aqueous and immersion liquid (n around 1.465) solutions using water- and oil-immersion objectives. We also determined the effect on lateral resolution by imaging 0.1-μm fluorescent microspheres.

2 Materials and Methods

The multiphoton imaging system used in this study is the LSM 510 META (Zeiss, Germany) coupled to a femtosecond

Address all correspondence to Chen Yuan Dong, Department of Physics, National Taiwan University, No. 1, Sec. 4, Roosevelt Rd. Taipei 106, Taiwan. Tel: 886-2-33665155; FAX: 886-2-33665244; E-mail: cydong@phys.ntu.edu.tw

1083-3668/2008/13(4)/044023/6/$25.00 © 2008 SPIE

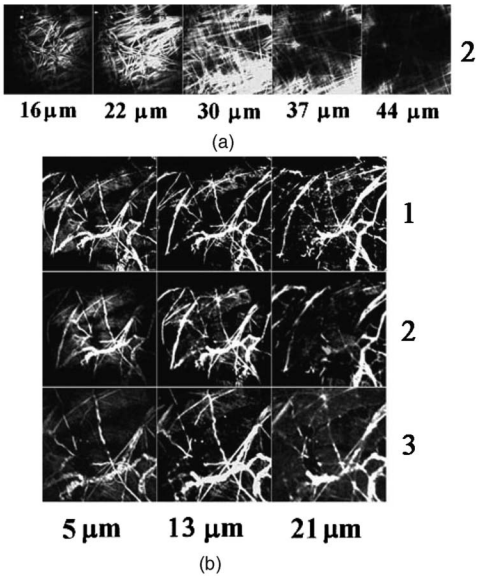

Fig. 1 SHG images of chicken leg fasciae at different imaging depths. 1: C-Apochromat 40×/NA 1.2 W; 2: Fluar 40×/NA 1.3 oil; 3: Plan-Apochromat 63×/NA 1.4 oil. Frame size 1 and 2: 325×325 μm^2; 3: 206×206 μm^2.

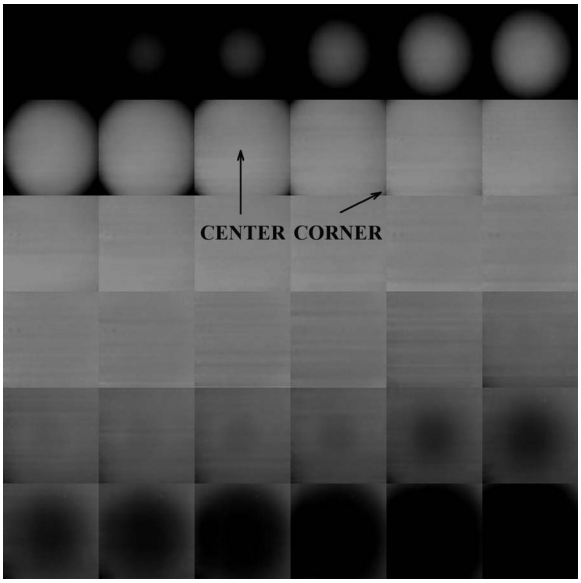

Fig. 2 Depth-dependent SRB TPF images. Single frame size-325 ×325 μm^2. Objective 2 (Fluar 40×/NA 1.3 oil).

titanium:sapphire laser operating at 780 nm (Tsunami, Spectra-Physics, Mountain View, California). Three-high-numerical-aperture Zeiss objectives of the water immersion type (objective 1: C-Apochromat 40×/NA 1.2 W Corr) and oil immersion [objective 2: Fluar 40×/NA 1.3; ojective 3: Plan-Apochromat 63×/NA 1.4 differential interference contrast (DIC)] were used. To investigate the effects of the field inhomogeneity in multiphoton imaging, uniform 10-μM SRB solutions in water and immersion liquid (IL) (refractive index n around 1.465 at 780 nm from Cargille Laboratories) were used. Low concentration SRB samples were prepared by dilution of the 10-mM SRB stock solution [in phosphate buffered saline (PBS)] with water and the IL. The variation of the point spread function (PSF) across the imaging field was determined by imaging 0.1-μm green fluorescent microspheres (64010-15, Molecular Probes Incorporated, Eugene, Oregon) imbedded in agarose gel. The method for sample preparation and PSF measurement was similar to that previously described.[6] For SHG imaging, fascia samples isolated from chicken leg were used. The SHG and TPF signals were respectively detected in the 380 to 400-nm and 435 to 700-nm spectral regions in a backward geometry. Finally, ImageJ was used for image processing.

3 Results and Discussion

3.1 *Second Harmonic Generation Demonstration of Lateral Image Inhomogeneity*

To demonstrate the field inhomogeneity in multiphoton imaging, the SHG images of thin segments of chicken leg fascia were obtained at different imaging depths using the three objectives. Fascia consists of parallel and interlaced collagen fibers (mainly of type 1), which produce intensive second harmonic generation signal from pulsed, IR laser irradiation were imaged. For fascia SHG imaging with the oil-immersion objective 2 (Fluar 40×/NA 1.3), images at depths of 16 and 22 μm show that the collagen fibers at the center of the images are more intense than those at the peripheral region [Fig. 1(a)]. At the imaging depth of 30 μm, comparable intensity across the entire frame was observed. However, at the greater imaging depths of 37 and 44 μm, the fibers at the image center become darker than those in the peripheral region. In addition to the existence of off-axis image inhomogeneity, these SHG images reveal that up to a depth of 30 μm, the fibers located at the central part of the imaging field tend to become increasingly intense with imaging depths. This phenomenon is demonstrated by the horizontally oriented fibers of the fasciae sample in Fig. 1(b), series 2. In the case of the two Apochromat-type objectives (objective 1: C-Apochromat 40×/NA 1.2 W, and objective 3: Plan-Apochromat 63/NA 1.4 oil), this phenomenon is less prominent [Fig. 1(b), series 1 and 3].

3.2 *Qualitative and Quantitative Characterization of Lateral Image Inhomogeneity*

While the existence of off-axis image inhomogeneity was revealed by the SHG imaging of chicken leg fasciae using oil-immersion objective 2 (Fluar 40×/NA 1.3 oil), uniform fluorescent SRB samples were used to quantify this effect across the two-photon imaging field. Portions of the axial images of the aqueous SRB sample (thickness ~70 μm, frame size 325×325 μm^2), acquired with the same objective (Fluar 40×/NA 1.3 oil) are shown in Fig. 2. The corresponding depth dependence of the axial intensity is shown in Fig. 3. For calculating the intensity profile along the optical axis, a circular region 10 μm in diameter located at the frame center was selected. For peripheral region analysis, two circular regions of the same size were selected at the opposite corners of the image frame located 220 μm away from the frame center. From Figs. 2 and 3, it is evident that the focal points of the

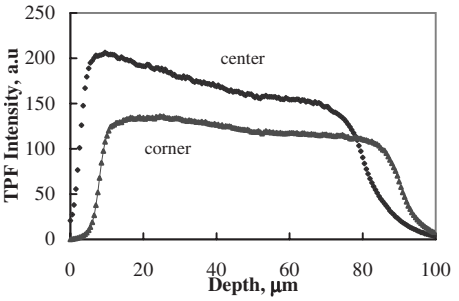

Fig. 3 Axial profiles of SRB TPF intensity at the frame center and corners (see Fig. 2).

scanning laser form a convex surface with its top located approximately at the center of the scanning field.

For additional quantitative analysis, the derivatives of the axial intensity profiles obtained by the oil-immersion objective 2 (Fluar 40×/NA 1.3 oil) were computed and plotted with peak width [full width at half maximum (FWHM)] characterizing the integrated TPF axial response (IAR). Figure 4(a) illustrates that the maxima and minima of the curves correspond respectively to the axial positions of the front and back sample surfaces. The peripheral focal points 220 μm away from the center fall behind the central focal points by $\Delta Z_{front}=Z_{max,corner}-Z_{max,center}=4.9$ μm. At the back surface (~70 μm below the front surface), this value increased to $\Delta Z_{back}=Z_{min,corner}-Z_{min,center}=7.9$ μm. The IAR increased from 1.9 μm at the center of the image frame to 2.8 μm at the corner (increase of 147%). At a depth of 70 μm, the respective IARs at the center and corner are 7.0 and 7.8 μm. For comparison, the axial SRB TPF profiles were determined with the water-immersion objective 1 (C-Apochromat 40×/NA 1.2 W). The derived curves [Fig. 4(b)] show a much smaller concavity of the scanning surface. At last for the well-corrected oil-immersion objective 3 (Plan-Apochromat 63×/NA 1.4 oil), a flat scanning surface was observed (Table 1).

To further investigate the field inhomogeneity in multiphoton imaging, additional image analysis was performed for the three objectives using 10-μM SRB dissolved in a solution with a higher refractive index immersion liquid (IL, n around 1.465). The results show that the IARs of the lateral image inhomogeneity effect at the front surface depend on the objective type (Table 1). However, when the field inhomogeneity is present, it strongly depends on RIM and image depth [Fig. 4(a)].

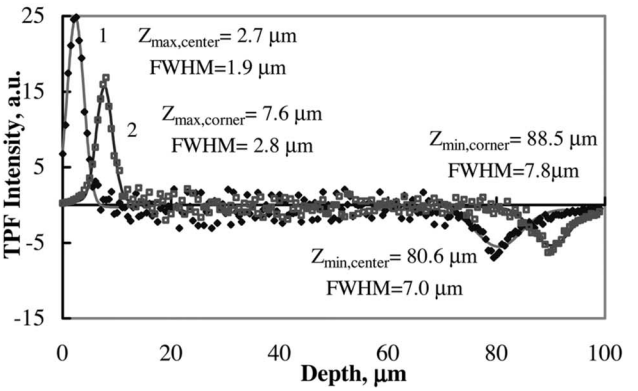

(a)

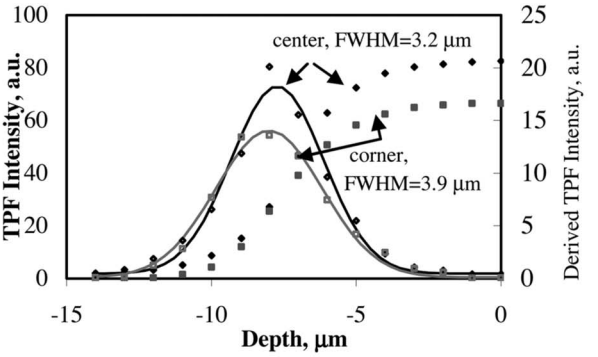

(b)

Fig. 4 (a) Derivatives of aqueous SRB axial intensity profiles (see Fig. 3). 1 is the frame center, and 2 is the frame corner (smooth curves-Gaussian fits). Objective 2: Fluar 40×/NA 1.3 oil. (b) Axial profiles and the corresponding derivatives for aqueous SRB TPF intensity (smooth curves-Gaussian fits). Objective 1: C-Apochromat 40× NA 1.2 W corr.

3.3 *Investigation of Depth-Dependent Lateral Profiles*

To compare the depth-dependent image inhomogeneity effects, at image surface and at depths of 75 and 120 μm, lateral profiles of the uniform SRB samples in water [Fig. 5(a)]

Table 1 Integral TPF axial response (IAR) in the image frame centers and corners along with the relative axial shifts (in micrometers).

	Water n = 1.33			Immersion liquid n = 1.465		
Objective	Center	Corner	ΔZ_{front}	Center	Corner	ΔZ_{front}
1: C-Apochromat 40× NA1.2 W corr	3.2	3.9	−0.35	2.9	3.6	−0.3
2: Fluar 40×/NA 1.3 oil	1.9	2.8	4.9	2	2.9	5.0
3: Plan-Apochromat 63×/NA1.4 oil DIC	2.0	2.3	0.0	2.1	2.4	0.0

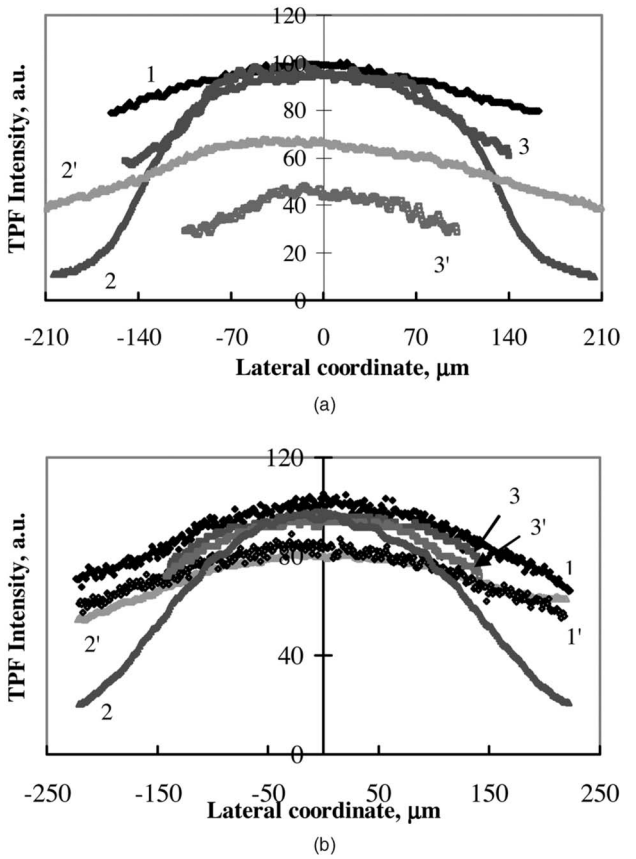

Fig. 5 Lateral profiles of SRB TPF at the surface (1, 2, 3) and at the depths of 120 μm (1′,2′) and 75 μm (3′). (a) Aqueous solution. (b) Immersion liquid. n around 1.465. 1 and 1′ are objective 1: C-Apochromat 40× NA 1.2 W corr; 2 and 2′ are objective 2: Fluar 40×/NA 1.3 oil; and 3 and 3′ are objective 3: Plan-Apochromat 63×/NA 1.4 oil DIC.

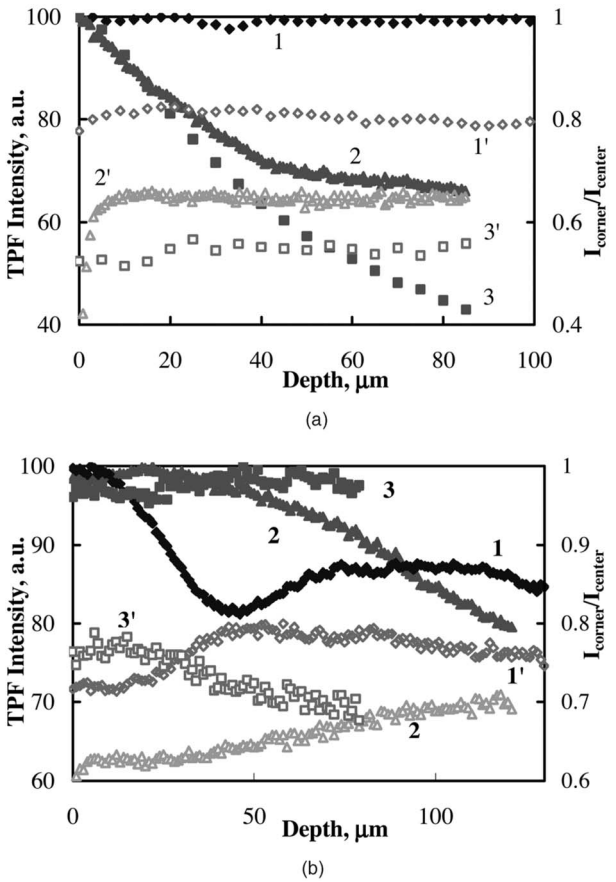

Fig. 6 Axial profiles of SRB TPF intensity in the frame center (1, 2, and 3, left *y* axis) and the intensity ratio from the corner to the center (1′, 2′, and 3′, right *y* axis). (a) Aqueous solution and (b) immersion liquid. n around 1.465. 1 and 1′ are objective 1: C′-Apochromat 40 × NA 1.2 W corr; 2 and 2′ are objective 2: Fluar 40×/NA 1.3 oil, and 3 and 3′ are objective 3: Plan-Apochromat 63×/NA 1.4 oil DIC.

and IL [Fig. 5(b)] at the two depths have been plotted. In addition, comparison between the axial profiles in the central and peripheral regions (Fig. 6) was made for the two fluorescent SRB samples. For plotting the lateral profiles, a rectangular region 4 μm wide along the frame diagonal was chosen. For plotting the axial profiles, a circular region 4 μm in diameter was selected at the frame center and corner (~227 μm away from the center for objectives 1 and 2 and 140 μm for objective 3). The results show that in using the water-immersion objective 1 (C-Apochromat 40×/NA 1.2 W) for imaging the aqueous SRB specimen, lateral profiles at a depth of 120 μm (data not shown) are very similar to those at the surface [Fig. 5(a)]. The lateral intensity profile 140 μm away from the center decreases by less than 15% [Fig. 5(a)] and no intensity decay in the axial direction is observed [Fig. 6(a)]. These results suggest that objective 1 is well corrected for aqueous samples with 170-μm cover glass and that the axial degradation is negligibly small for 0 to 100 μm depth.

However, for the oil-immersion objectives, when RIM is essential for the aqueous samples, our results reveal that lateral intensity degraded more than 40% from center to corner [Fig. 5(a)], and more than 35 and 50% of degradation from surface to the depth of 80 μm were respectively observed for objective 2 (Fluar 40×/NA 1.3 oil) and objective 3 (plan-Apochromat 63×/NA 1.4 oil) [Fig. 6(a)]. More importantly, for objective 2, the image with maximum intensity heterogeneity was observed at the sample surface [Figs. 5(a) and 5(b)]. This large nonuniformity can be explained by the axial shift of the focal point axial coordinate at the corner away from that of the center [Fig. 4(a)]

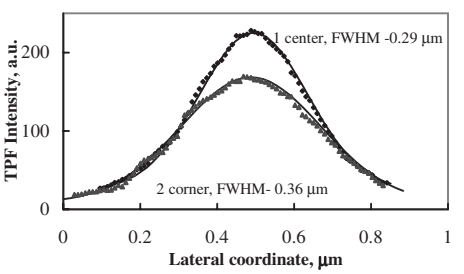

Fig. 7 Lateral TPF intensity profiles of 0.1-μm fluorescent beads near the water-agarose sample surface and FWHM of PSF at center (1) and corner (2) of the frame (smooth curves—Gaussian fits). Objective 2: Fluar 40×/NA 1.3 oil.

Table 2 Lateral PSF FWHMs in the water-agarose sample at different locations (in micrometers).

	Surface			80 μm depth		
Localization Objective	1 center	2 corner	2/1, %	1 center	2 corner	2/1, %
1: C-Apochromat 40× NA1.2 W corr	0.33	0.39	118	0.34	0.4	118
2: Fluar 40×/NA1.3 oil	0.28	0.36	129	0.34	0.43	126
3: Plan-Apochromat 63×/NA1.4 oil DIC	0.29	0.37	128	0.38	0.48	126

As Figs. 5 and 6 illustrate, the image lateral inhomogeneity effects exist for both oil- and water-immersion objectives in IL with refractive index of around 1.465 as well. The effects in the imaging field are similar to those for the aqueous sample whose refractive index is n=1.33 (Fig. 5). However, the results for the axial profiles were very different. In Fig. 6(b), for the two oil-immersion objectives, up to a depth of 60 μm, a small signal loss was observed in the immersion liquid (curves 2 and 3), compared with the aqueous medium [Fig. 6(a)]. Thus, the oil-immersion objectives can be used to obtain uniform TPF signals along depths throughout much of the working distance in samples with refractive indexes of around 1.465. For the water-immersion objective, a nonmonotonous intensity decay profile was observed [Fig. 6(b), curve 1]. This observation may be caused by the excitation light passing through media with three different refractive indexes 1.33 (water), 1.515 (cover glass), and around 1.465 (immersion fluid) in reaching the focal point.

3.4 *Off-Axis Broadening of Lateral Point Spread Function*

As a final characterization of the 3-D image inhomogeneity, the lateral PSF was measured for the three objectives at different depths. For measuring the lateral PSF in the central region, four to five fluorescent beads inside a 10-μm diameter circular region at the frame center were chosen. For the off-axis measurement, the beads were selected at approximately 140 μm away from the center. The PSF characterization results are shown in Fig. 7 and Table 2.

The physical reason for causing the 3-D image heterogeneity in multiphoton scanning of uniformly luminescent specimens can be numerous. Factors associated with change of the laser beam intensity along any coordinate, such as reduction of entrance aperture for inclined beams, increase of Fresnel losses, and total internal reflection on borders of mediums with different refractive indexes at larger scanning angles, absorption, and scattering of excitation and emission radiation can all contribute. Furthermore, the broadening of the PSF and shifting of focal position involving RIM at interfaces of media with different indices of refraction (immersion liquid/cover-glass/sample) can lead to shifts of the axial focal spot positions), which results in the distortion of geometrical form of specimen, reduction of image resolution, and loss in signal intensity level.

Regarding high numerical aperture objectives, when a paraxial ray refracts at interfaces of two media with different refractive indexes, the shifted axial and lateral focal positions induced a defocused laser beam, as illustrated in Fig. 8.

Suppose that the effect of spherical aberration is not present, that is, when the refractive index (n_i) of the immersion liquid or cover glass is equivalent to the refractive index (n_s) of the sample, $d(d')$ is the crossing point of approxi-

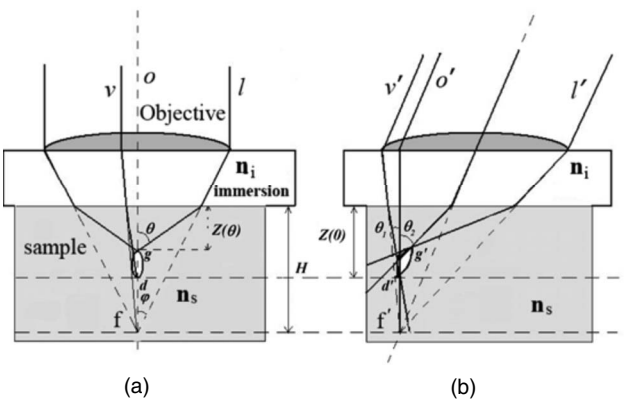

Fig. 8 Effects of refractive index mismatch on focal spots with (a) excitation parallel, and at (b) an inclination angle to the optical axis ($n_i > n_s$).

mately vertical rays $v(v')$ whose focal point is positioned at $f(f')$ with axial position at H. In the case that $n_i > n_s$, the crossing point of the rays $l(l')$ and $o(o')$ becomes $g(g')$. The coordinate of such a crossing point is $Z(\theta)$ and depends on the inclination angle. Note that at θ, defocus can take place within the limits of $\Delta Z = Z(0) - Z(\theta) = H(\sin\theta \sin\varphi - \tan\theta/\tan\varphi)$. As the laser beam enters the objective, an additional dithering of PSF focal volume shown in Fig. 8(b) can occur. In addition, due to the fact that $\theta_2 > \theta, g'$ is located above g and PSF is more extended in the axial direction [Fig. 8(a)]. These effects may contribute to the multiphoton image field inhomogeneity effects.

4 Conclusion

The unique 3-D imaging capabilities of multiphoton microscopy have been successfully applied in imaging micron-sized objects such as cells, neuron fibers, and other tissues. However, aberration effects can contribute to the degradation of detected intensity and spatial resolution. In the past, researchers have investigated PSF enlargement along the axial direction, the corresponding decrease of resolution, and the attenuation of signals caused by spherical aberration induced by RIM.[2–8] However, image degradation resulting from off-axis imaging, to the best of our knowledge, has not been investigated. In this study, the extent of lateral image inhomogeneity effects in two-photon and SHG microscopy are examined. Both the convexity of the scanning surface and radial PSF degradation are investigated in the presence of different RIM (using different immersion liquids and samples with different refractive indexes). Our results show that these effects depend on refractive index mismatch, and need to be accounted for in both qualitative and quantitative multiphoton applications.

Acknowledgments

We would like to acknowledge the research support provided by the National Research Program for Genomic Medicine (NRPGM), National Science Council of Taiwan. This project was completed in the Optical Molecular Imaging Microscopy Core Facility (A5) of NRPGM. We would also like to thank Shu-Jen Chiang for editorial assistance.

References

1. W. Denk, J. H. Strickler, and W. W. Webb, "Two-photon laser scanning fluorescence microscopy," *Science* **248**(4951), 73–76 (1990).
2. S. Hell, G. Reiner, C. Cremer, and E. H. K. Stelzer, "Aberrations in confocal fluorescence microscopy induced by mismatches in refractive index," *J. Microsc.* **169**(3), 391–405 (1993).
3. G. J. de Grauw, J. M. Vroom, H. T. M. van der Voort, and H. C. Gerritsen, "Imaging properties in two-photon excitation microscopy and effects of refractive-index mismatch in thick specimens," *Appl. Opt.* **38**(28), 5995–6003 (1999).
4. A. K. Dunn, V. P. Wallace, M. Coleno, M. W. Berns, and B. J. Tromberg, "Influence of optical properties on two-photon fluorescence imaging in turbid samples," *Appl. Opt.* **39**(7), 1194–1201 (2000).
5. M. J. Booth and T. Wilson, "Refractive-index-mismatch induced aberrations in single-photon and two-photon microscopy and the used of aberration correction," *J. Biomed. Opt.* **6**(3), 266–272 (2001).
6. C. Y. Dong, K. Koenig, and P. So, "Characterizing point spread functions of two-photon fluorescence microscopy in turbid medium," *J. Biomed. Opt.* **8**(3), 450–459 (2003).
7. C. K. Tung, Y. Sun, W. Lo, S. J. Lin, S. H. Jee, and C. Y. Dong, "Effects of objective numerical apertures on achievable imaging depths in multiphoton microscopy," *Microsc. Res. Tech.* **65**(6), 308–314 (2004).
8. C. Y. Dong, B. Yu, P. D. Kaplan, and P. T. C. So, "Performances of high numerical aperture water and oil immersion objective in deep-tissue, multi-photon microscopic imaging of excised human skin," *Microsc. Res. Tech.* **63**(1), 81–86 (2004).
9. J. Roerdink and M. Bakker, "An FFT-based method for attenuation correction in fluorescence confocal microscopy," *J. Microsc.* **169**(1), 3–14 (1993).
10. A. Liljeborg, M. Czader, and A. Porwit, "A method to compensate for light attenuation with depth in 3D DNA image cytometry using a confocal scanning laser microscope," *J. Microsc.* **177**(2), 108–114 (1995).
11. C. Kervrann, D. Legland, and L. Pardini, "Robust incremental compensation of the light attenuation with depth in 3D fluorescence microscopy," *J. Microsc.* **214**(3), 297–314 (2004).
12. S. C. Lee and P. Bajcsy, "Intensity correction of fluorescent confocal laser scanning microscope images by mean-weight filtering," *J. Microsc.* **221**(2), 122–136 (2006).
13. A. Can, O. Al-Kofahi, S. Lasek, D. H. Szarowski, J. N. Turner, and B. Roysam, "Attenuation correction in confocal laser microscopes:a novel two-view approach," *J. Microsc.* **211**(1), 67–79 (2003).
14. W. Lo, Y. Sun, S. J. Lin, S. H. Jee, and C. Y. Dong, "Spherical aberration correction in multiphoton fluorescence imaging using objective correction collar," *J. Biomed. Opt.* **10**(3), 034006 (2005).
15. M. Schwertner, M. J. Booth, and T. Wilson, "Characterizing specimen induced aberrations for high NA adaptive optical microscopy," *Opt. Express* **12**(26), 6540–6552 (2004).
16. M. Rueckel, J. A. Mack-Bucher, and W. Denk, "Adaptive wavefront correction in two-photon microscopy using coherence-gated wavefront sensing," *Proc. Natl. Acad. Sci. U.S.A.* **103**(46), 17137–17142 (2006).